ELSEVIER

Journal of Non-Crystalline Solids 265 (2000) 19–28

JOURNAL OF NON-CRYSTALLINE SOLIDS

www.elsevier.com/locate/jnoncrysol

Effects of Eu_2O_3 on liquid–liquid phase separation of $PbO–B_2O_3$, $BaO–B_2O_3$ and $SrO–B_2O_3$ glasses

Tomoya Konishi [a,*], Tomoyoshi Asano [a], Yuu Ishii [a], Kohei Soga [a], Hiroyuki Inoue [a], Akio Makishima [a], Satoru Inoue [b]

[a] *Department of Materials Science, School of Engineering, The University of Tokyo, 7-3-1, Hongo, Bunkyo-ku, Tokyo 113-8656, Japan*
[b] *National Institute for Research in Inorganic Materials, Namiki 1-1, Tsukuba, Ibaraki 305-0044, Japan*

Received 26 July 1999; received in revised form 3 November 1999

Abstract

The effects of Eu_2O_3 on liquid–liquid phase separation were studied in the $RO–B_2O_3–Eu_2O_3$ (R represents Pb, Ba or Sr) systems. The results from the in situ observation of the phase separation showed that, in every case, Eu_2O_3 addition increased the immiscibility temperatures and the effect was more pronounced as the RO content decreased. The Eu distribution in the phase-separated microstructure was examined with an electron probe microanalyser (EPMA) and a field emission scanning electron microscope (FE-SEM) with an energy dispersive X-ray spectrometer (EDS). It was found that the Eu dissolved preferentially in the RO-rich phase droplets with a uniform distribution. A comprehensive account for these effects of Eu_2O_3 on both the immiscibility temperature and the microstructure was given by considering the $RO–B_2O_3–Eu_2O_3$ ternary phase diagram. For the $SrO–B_2O_3–Eu_2O_3$ system, the Eu_2O_3 concentration in the droplets was measured with EDS analysis to be found adjustable by changing batch composition.

PACS: 81.05.Kf; 64.75.1g; 07.79.2v

1. Introduction

Liquid–liquid phase separation is a phenomenon in which a uniform molten glass decomposes into two liquid phases when heat-treated at a temperature below an immiscibility boundary. Alkaline earth borate glasses are typical examples precipitating droplets of hundreds of nanometers to tens of micrometers in diameter dispersed in a matrix. So far a number of studies have been conducted on the liquid–liquid phase separation in alkaline earth borate systems and the $PbO–B_2O_3$ system in terms of microstructure [1], immiscibility temperature [2–8], phase separation rate measured by in situ observation under gravity [7,8] or micro gravity [9], as well as calculations based on thermodynamic theories [10–13].

Liquid–liquid phase separation is potentially applicable to produce glasses with new functions as mentioned by Inoue et al. [14]. A microsphere obtained from phase separation of glass can be used as a micro lens or a micro optical glass

* Corresponding author. Tel.: +81-3 5841 7117; fax: +81-3 5841 8653.
E-mail address: kon@glass.mm.t.u-tokyo.ac.jp (T. Konishi).

0022-3093/00/$ - see front matter
PII: S0022-3093(99)00878-9

resonator [15,16] by morphology-dependent resonances. It is also possible to obtain crystal-dispersed glasses by crystallizing precipitated droplets. Elongation of droplets by pulling or pressing glass makes the glasses optically anisotropic [17]. Moreover, phase-separated glass containing nano-size droplets may act as 'laser paint' which has a resonance effect resulting from strong light scattering [18].

Also phase-separated droplets may be used as micro containers to embed elements enabling new properties and functions in glasses, because two decomposed phases are different in their solubility of a certain elements as well as in their compositions. For example, the introduction of rare earth elements is used to give glasses functions like fluorescence light emission. Such a case was reported by Yao et al. on phase separation of sodaborosilicate glass containing Eu where Eu was estimated to exist mainly in the sodaborate-rich phase from its emission intensity ratio [19].

In order to design such processes systematically, it is necessary to obtain knowledge on the influence of rare earth dopants on phase separation from the aspects of (a) the immiscibility boundary and (b) the distribution of rare earth elements in the whole microstructure and each phase in products obtained. The immiscibility boundary is essential for developing proper heat-treatment schedules. The distribution of rare earth elements is important for optical materials, since luminescence emission properties of rare earth elements are dependent on the surrounding matrix.

In this study, we investigated how the addition of Eu_2O_3 changed the liquid–liquid immiscibility temperatures and modified the microstructure of the $PbO–B_2O_3$, $BaO–B_2O_3$ and $SrO–B_2O_3$ systems, utilizing an in situ observation technique. The Eu element distribution in the whole microstructure and in each phase after proper heat-treatments was measured by an electron probe microanalyser (EPMA) or a field emission scanning electron microscope with an energy dispersive X-ray spectrometer (FE-SEM/EDS).

2. Experimental

2.1. Preparation of the samples

The glasses of the systems $PbO–B_2O_3$ with Eu_2O_3, $BaO–B_2O_3$ with Eu_2O_3, and $SrO–B_2O_3$ with or without Eu_2O_3 were prepared by a melt-quench method. The batch compositions are listed in Table 1. As for the systems $BaO–B_2O_3$ and $SrO–B_2O_3$, in situ observation was possible in the composition range on the B_2O_3-rich side of the immiscibility dome. In the composition range on the B_2O_3-poor side of the dome, the precipitation of droplets was not observed but quick decomposition into two layers occurred under gravity [9]. The batch for each glass was prepared as the mixture of reagents weighed suitably for the composition. The batch was melted in a Pt crucible at a temperature higher than the immiscibility temperature in an electric furnace and held at the temperature for one or a half an hour to obtain a homogeneous mixture. The melt was quenched to a glassy frit by squeezing it between two carbon blocks. The reagents we employed and the batch melting conditions are listed on Table 2. Changes in the compositions of $1BaO \cdot 99B_2O_3$ (mol%) and $5BaO \cdot 95B_2O_3$ (mol%) glasses during melting were analysed with an inductively coupled plasma (ICP) spectrometry technique by Inoue et al. [8] to be found negligible for the following experiments.

2.2. In situ observation of the phase separation process

Measurements of liquid–liquid immiscibility boundaries of the systems with an in situ observation technique was made by Inoue et al. on the systems $PbO–B_2O_3$ [7] and $BaO–B_2O_3$ [8] without Eu_2O_3. We employed the identical apparatus for the in situ observations reported here in order to follow the same procedures. About 0.4 g amount of as-quenched glass was put in a 13 mm$\varnothing$ Pt pan and set in the electric furnace for the in situ observation. The sample was initially heated up to a temperature higher than the immiscibility temperature, and held at the temperature for 3 min to form a uniform melt. The melt was cooled down to

Table 1
Batch compositions of the glass samples

Glass	Base composition		Eu_2O_3 addition		In situ obs.	Eu analyses
	mol%	wt%	mol%	wt%		
A	$1.3PbO \cdot 98.7B_2O_3$	$4.0PbO \cdot 96.0B_2O_3$	0.084	0.40		○
B	$3.4PbO \cdot 96.6B_2O_3$	$10PbO \cdot 90B_2O_3$	0.021	0.10	○	
C			0.042	0.20	○	
D	$7.2PbO \cdot 92.8B_2O_3$	$20PbO \cdot 80B_2O_3$	0.023	0.10	○	
E			0.046	0.20	○	
F	$12PbO \cdot 88B_2O_3$	$30PbO \cdot 70B_2O_3$	0.025	0.10	○	
G			0.050	0.20	○	
H	$17PbO \cdot 83B_2O_3$	$40PbO \cdot 60B_2O_3$	0.027	0.10	○	
I			0.055	0.20	○	
J	$1.0BaO \cdot 99.0B_2O_3$	$2.2BaO \cdot 97.8B_2O_3$	0.10	0.50	○	
K			0.20	1.0	○	
L	$3.0BaO \cdot 97.0B_2O_3$	$6.4BaO \cdot 93.6B_2O_3$	0.10	0.50	○	
M			0.20	1.0	○	
N			0.50	2.5	○	○
O	$5.0BaO \cdot 95.0B_2O_3$	$10BaO \cdot 90B_2O_3$	0.1	0.50	○	
P			0.21	1.0	○	
Q	$0.50SrO \cdot 99.50B_2O_3$	$0.74SrO \cdot 99.26B_2O_3$	–	–	○	
R			0.050	0.25	○	○
S	$1.0SrO \cdot 99.0B_2O_3$	$1.5SrO \cdot 98.5B_2O_3$	–	–	○	
T			0.050	0.25	○	○
U	$1.5SrO \cdot 98.5B_2O_3$	$2.2SrO \cdot 97.8B_2O_3$	–	–	○	
V			0.050	0.25	○	○
W	$2.0SrO \cdot 98.0B_2O_3$	$2.9SrO \cdot 97.1B_2O_3$	–	–	○	
X			0.050	0.25	○	○
Y	$2.5SrO \cdot 97.5B_2O_3$	$3.7SrO \cdot 96.3B_2O_3$	–	–	○	
Z			0.050	0.25	○	○

Table 2
Batch melting conditions

System	Reagents	Crucible	Melting temperature (°C)	Melting time (min)
$PbO–B_2O_3$	PbO, H_3BO_3	Pt	950	30
$BaO–B_2O_3$	$BaCO_3$, H_3BO_3	Pt	1200	60
$SrO–B_2O_3$	$SrCO_3$, H_3BO_3	Pt	1350	60

the liquidus temperature at a rate of 2.5°C/min, simultaneously being observed by a charge coupled device (CCD) camera through a silica window attached to the top of the furnace. The pictures were recorded on videotape for later analyses.

Under the above conditions, the phase separation in the $PbO–B_2O_3$ system is perceived as darkening in the visual field due to the strong light scattering by the droplets precipitated which are too small to be identified separately. Inoue et al. [7] determined the temperatures, T_1 and T_2, at which the darkening began and completed, respectively, as criteria for estimating the immiscibility temperature. We also determined T_1 and T_2 of the $PbO–B_2O_3$ system with Eu_2O_3 addition for comparison.

On the other hand, in the $BaO–B_2O_3$ and $SrO–B_2O_3$ systems, the precipitation of individual droplets is detectable under the above conditions. Inoue et al. [8] determined the temperature T_p at which the onset precipitation was first detected within the visual field. We followed the same procedure for the systems with Eu_2O_3 addition for comparison.

In these procedures, the immiscibility temperature are estimated only from the darkening temperature (T_1, T_2) or the onset precipitation temperature (T_p) during cooling which is susceptible to an error from undercooling. For the PbO–B_2O_3 system, Inoue et al. [7] reported that the immiscibility temperatures reported by other researchers [3,10,11] were in between T_1 and T_2, which indicates that the error could be negligible. For the system BaO–B_2O_3, the comparison between the result from these procedures and that from the temperature gradient furnace method [3], which enables the measurement in equilibrium, was discussed [8]. The error decreased with the decreasing BaO content; it was about 50°C for the $5BaO \cdot 95B_2O_3$ (mol%) and negligible for the composition with BaO less than 3 mol%. With respect to the system SrO–B_2O_3 system, since T_p had not been measured with the procedures yet, its correspondence with the immiscibility temperatures reported by other researchers [4–6] was verified prior to the measurement of T_p of the Eu_2O_3-doped SrO–B_2O_3 system.

2.3. Eu element-analyses of the phase separation structure

Samples were prepared by cooling the melt to room temperature at a rate of 2.5°C/min. The heat-treatment grew droplets large enough for EPMA and FE-SEM/EDS analyses of both the droplets and the matrix.

The phase-separated samples were crushed, and randomly selected pieces were fixed on the holders and coated with Au 200 Å in thickness by sputtering. The Eu distribution in the whole microstructure and in each phase was obtained with EPMA for the PbO–B_2O_3–Eu_2O_3 system and FE-SEM/EDS for the BaO–B_2O_3–Eu_2O_3 and SrO–B_2O_3–Eu_2O_3 systems.

The Eu_2O_3 concentration in the droplets was estimated by EDS analysis for the SrO–B_2O_3–Eu_2O_3 system. Prior to measurements, standard samples with different Eu_2O_3 contents were prepared to construct a standard calibration function correlating the specific X-ray (Eu Lα) signal intensity and the Eu_2O_3 content. The base composition of the standard samples were equivalent to the SrO-rich side end member compositions, $22SrO \cdot 78B_2O_3$ (mol%) which was almost the same as compositions of the obtained phase-separated droplets. The detected Eu Lα signal intensity in the droplets was converted into the Eu_2O_3 concentration based on the calibration function given by the above measurements on standard samples.

3. Results and discussion

3.1. Effect of Eu_2O_3 on the immiscibility temperatures

The temperatures T_1 and T_2 of the Eu_2O_3-doped PbO–B_2O_3 system and T_p of the Eu_2O_3-doped BaO–B_2O_3 and SrO–B_2O_3 systems were measured. In Figs. 1, 2 and 4, the data are superimposed on the RO–B_2O_3 binary phase diagrams as a function of a RO content to visualize the effect of Eu_2O_3 addition.

The temperatures T_1 and T_2 of the Eu_2O_3-doped PbO–B_2O_3 system are plotted with open markers

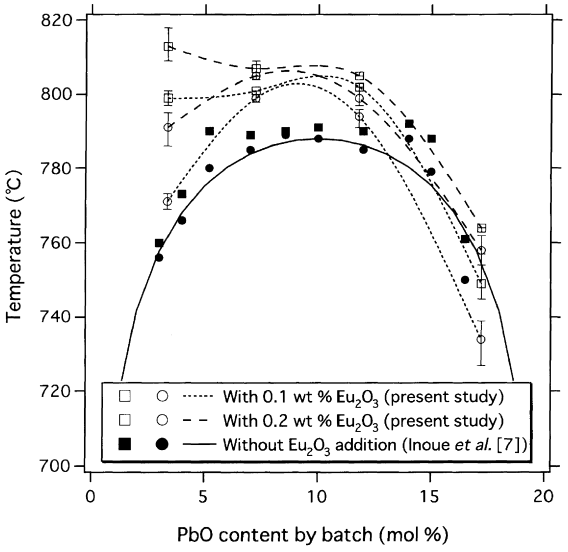

Fig. 1. Immiscibility temperatures of the PbO–B_2O_3 system with or without Eu_2O_3 addition. Square markers indicate T_1 and circle markers indicate T_2. Solid line shows the immiscibility boundary of the PbO–B_2O_3 system estimated from the Macedo and Simmons theory [10,11]. Broken lines are drawn as guides to the eye.

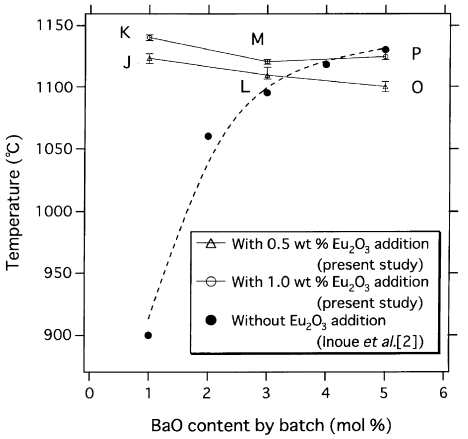

Fig. 2. Immiscibility temperatures of the $BaO–B_2O_3$ system with or without Eu_2O_3 addition. Single letters denote samples in Table 1. Lines are drawn as guides to the eye.

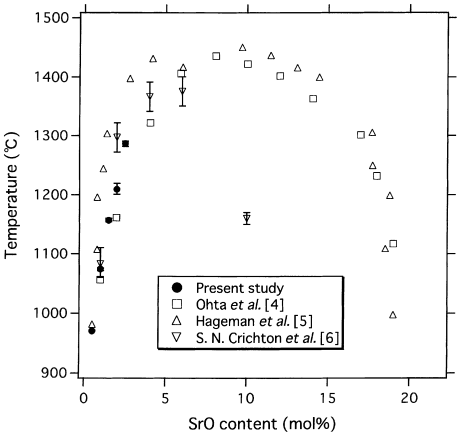

Fig. 3. Immiscibility temperatures of the $SrO–B_2O_3$ system.

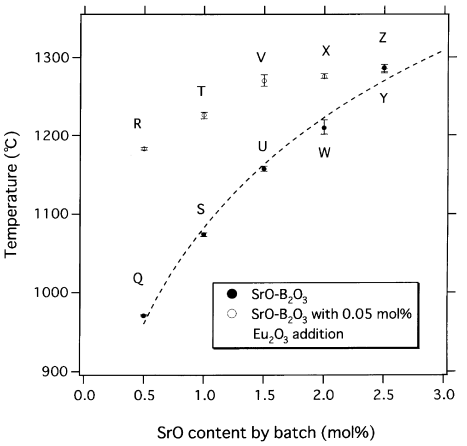

Fig. 4. Immiscibility temperatures of the $SrO–B_2O_3$ system with or without Eu_2O_3 addition. Line is drawn as a guide to the eye.

and error bars in Fig. 1. T_1 and T_2 measured on the samples without Eu_2O_3 addition by Inoue et al. [7] are also indicated by filled markers along with the immiscibility boundary estimated from the theory of Macedo and Simmons [10,11]. T_1 increased by about 50°C for Sample C by Eu_2O_3 addition. The T_1 and T_2 of Samples H and I are comparable to those of the Eu_2O_3-free samples.

With introduction of Eu_2O_3 to the $BaO–B_2O_3$ system, T_p increased by about 200°C where the BaO content was 2 mol %, as shown in Fig. 2. For the samples with more than 6 mol % BaO content, however, the Eu introduction had little effect on T_p.

The T_ps of Eu_2O_3-free $SrO–B_2O_3$ samples (Q, S, U, W, Y) in this study are plotted as filled markers and error bars in Fig. 3, while immiscibility temperatures reported by other researchers [4–6] are plotted as open markers. The obtained data were comparable to the other researchers' data, which implies that an error from undercooling could be negligible. Fig. 4 shows T_ps measured on the Eu_2O_3-doped samples (R, T, V, X, Z) together with those for the Eu_2O_3-free samples. For Sample R, T_p increased by 200°C. The difference between T_ps of Eu_2O_3-free and Eu_2O_3-doped samples decreased with the increasing SrO content, and became zero at 2.5 mol% SrO content.

In any system we investigated, the addition of Eu_2O_3 caused the immiscibility temperatures to rise significantly on the B_2O_3-rich side of the immiscibility domes by larger amount than the possible error from undercooling. In Figs. 1, 2 and 4, the data on the Eu_2O_3-doped samples are plotted on corresponding $RO–B_2O_3$ binary phase diagrams, despite their being ternary systems. To make things clearer for discussion, we have to consider ternary phase diagrams instead.

Fig. 5 shows schematically a ternary phase diagram of the $RO–B_2O_3–Eu_2O_3$ system with typical schematic results of the experiment. The data from the samples with a constant Eu_2O_3 content should be plotted on the Eu_2O_3-constant planes as

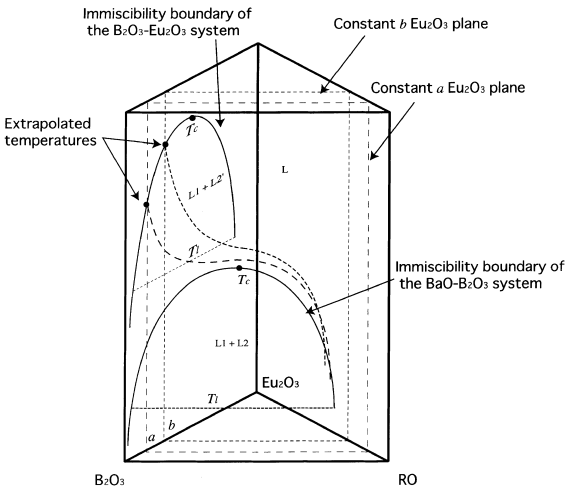

Fig. 5. Schematic ternary phase diagram of the $RO–B_2O_3–Eu_2O_3$ system.

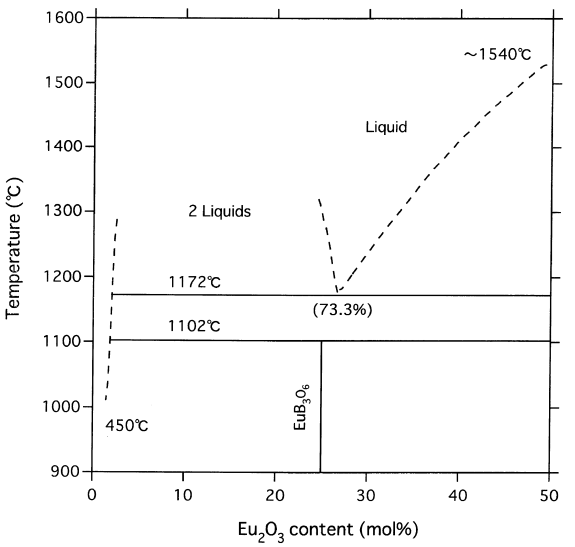

Fig. 6. Phase equilibrium diagram of the $Eu_2O_3–B_2O_3$ system reproduced from the literature [19].

denoted by the Eu_2O_3 content in Fig. 5. The planes correspond to the phase diagrams of the pseudo-binary $B_2O_3 \cdot xEu_2O_3–BaO \cdot yB_2O_3 \cdot x'Eu_2O_3$ system that both members contain Eu_2O_3. In the plane, the immiscibility temperature is extrapolated to a certain non-zero temperature at the $B_2O_3 \cdot xEu_2O_3$ end. The theory of Macedo and Simmons [10,11], which has successfully extended the concept of the binary regular mixing to that of the mixing of two stoichiometric oxides for the borate and silicate systems, requires that both ends should reach 0 K at end member compositions for the pseudo-binary phase separations. Thus the extrapolated non-zero temperatures suggest that, at least, the ternary system does not separate into $B_2O_3 \cdot xEu_2O_3$ and $BaO \cdot yB_2O_3 \cdot x'Eu_2O_3$ phases. From another point of view, it is also considered that the extrapolated non-zero temperature corresponds to a certain immiscibility temperature of the $Eu_2O_3–B_2O_3$ binary system. The concept of extrapolating immiscibility temperatures of a ternary system to the including binary system is general as is employed by Crichton et al. [6]. Fig. 6 shows the phase separation diagram of the $Eu_2O_3–B_2O_3$ binary system reproduced from the literature [20]. The diagram implies the presence of a two-liquid immiscibility dome though its boundary has not been determined yet. Therefore, it was considered that the immiscibility temperatures of the $RO–B_2O_3–Eu_2O_3$ ternary system with a smaller RO content were controlled by the immiscibility temperature of the $Eu_2O_3–B_2O_3$ binary system, resulting in the increase of the immiscibility temperatures by Eu_2O_3 addition in the B_2O_3-rich side of the miscibility gap. On the contrary, in the compositions where the RO content is relatively higher than the Eu_2O_3 content, the character of the phase separation in the $RO–B_2O_3$ binary system is dominant, resulting in a negligible effect of Eu_2O_3 addition.

3.2. Eu distribution in the liquid–liquid phase separation microstructure and the textures

Fig. 7 shows EPMA micrographs of Sample A. The back-scattered electron (BSE) image (a) shows the phase separation droplets which have grown up to about 20 μm in diameter by the heat-treatment. The Pb Lα image (b) and the Eu Lα image (c) of the same view are showing the shapes of phase separation droplets, which indicates that the droplets are rich in PbO and contain more Eu than the matrix. Fig. 8 shows a typical result of scanning the Pb Lα and Eu Lα intensities across a phase-separated droplet. Considering the signal noise level, the Pb and Eu

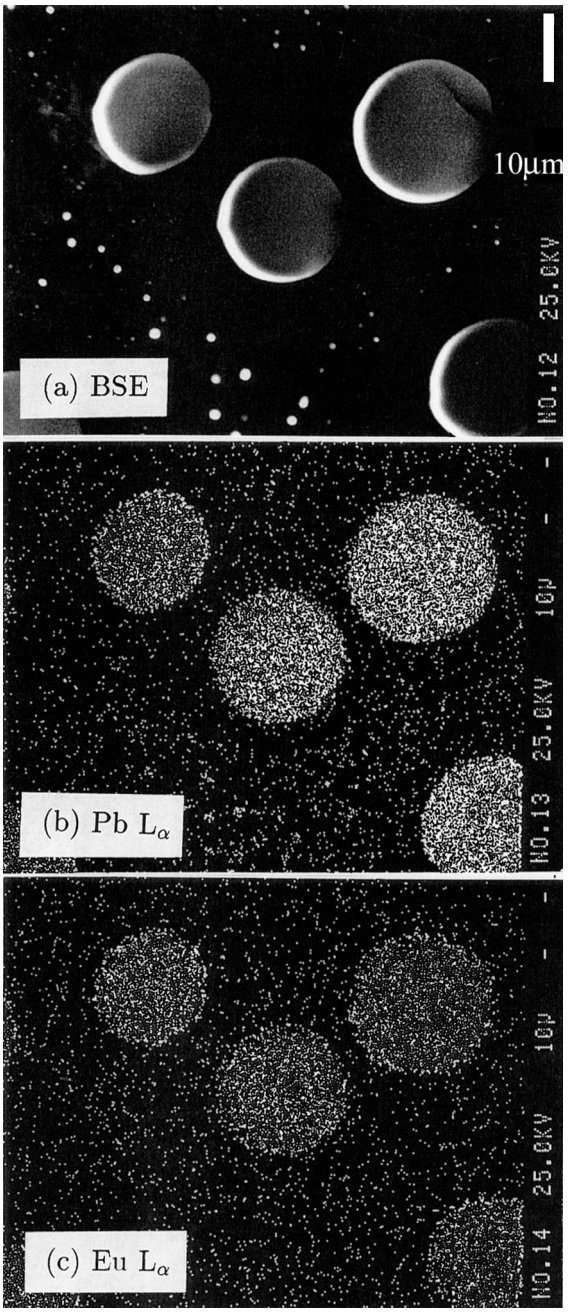

Fig. 7. Phase-separated microstructure observed with EPMA: (a) BSE image; (b) and (c) Pb Lα and Eu Lα intensity maps, respectively, in the same view as (a).

distribution in the droplet is almost flat which indicates that micro segregation of Eu was not caused on this scale.

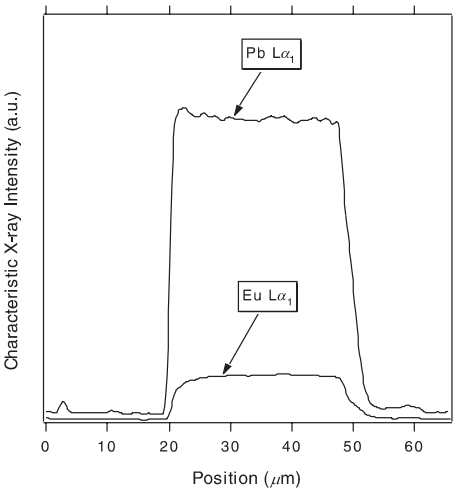

Fig. 8. Line scan analysis of Pb Lα and Eu Lα intensity across a phase-separated droplet of the $PbO–B_2O_3$ system.

Fig. 9(a) shows the fracture surface of an Eu_2O_3-doped phase separation texture of Sample N observed with FE-SEM. The picture shows that the B_2O_3 matrix has a porous texture while the droplets are dense, which implies that the droplets have better chemical durability than the matrix. Therefore, the use of droplets extracted from the microstructure is possible for applications such as micro lenses and optical resonators. No subsequent phase separation or crystallization was detected inside the droplet at a resolution of 1.6 nm. Fig. 9(b) and Fig. 9(c) show the characteristic X-ray intensity maps of Ba Lα and Eu Lα, respectively, detected with EDS area analyses on the same view. As is shown in Fig. 10, the same observation made on the $SrO–B_2O_3–Eu_2O_3$ system (Sample R) gave results similar to those of the $BaO–B_2O_3–Eu_2O_3$ system. In both cases, the Eu Lα signal intensity is high in the phase-separated droplet.

In any $RO–B_2O_3$ (R respects Pb, Ba or Sr) system, it was found that the Eu containing $RO–B_2O_3$ glasses separated completely into two phases; an almost pure B_2O_3 phase and a homogeneous RO-rich phase with Eu dissolved preferentially. This result supports the suggestion that the ternary system does not separate into $B_2O_3 \cdot xEu_2O_3$ and $BaO \cdot yB_2O_3 \cdot x'Eu_2O_3$ phases as was considered in

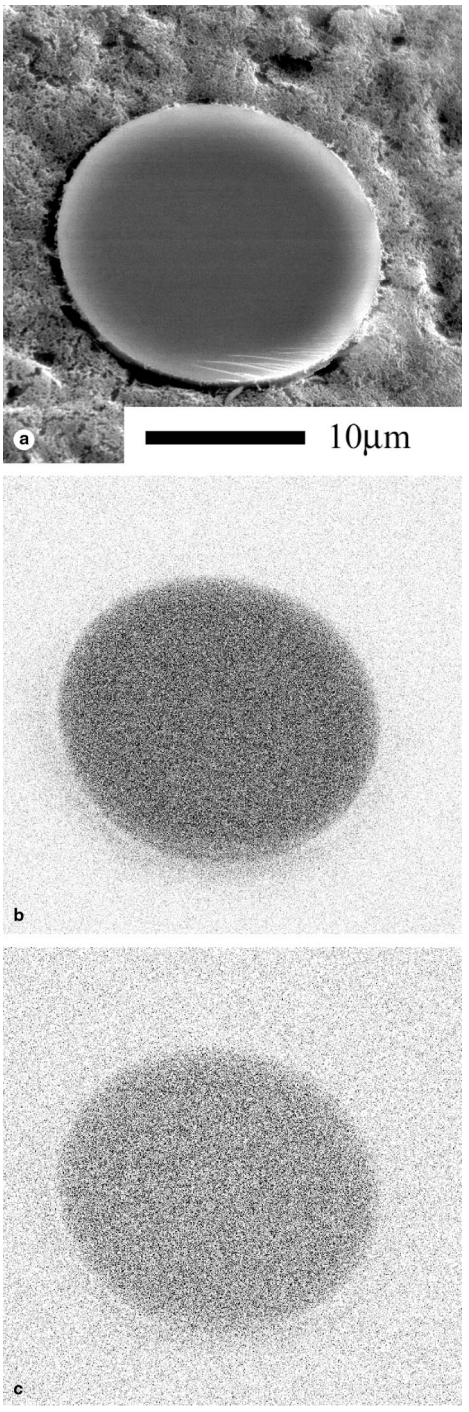

Fig. 9. (a) Fracture surface of an Eu_2O_3-doped phase-separated microstructure for Sample N observed with FE-SEM; (b) and (c) Ba Lα and Eu Lα intensity maps, respectively, in the same view as (a).

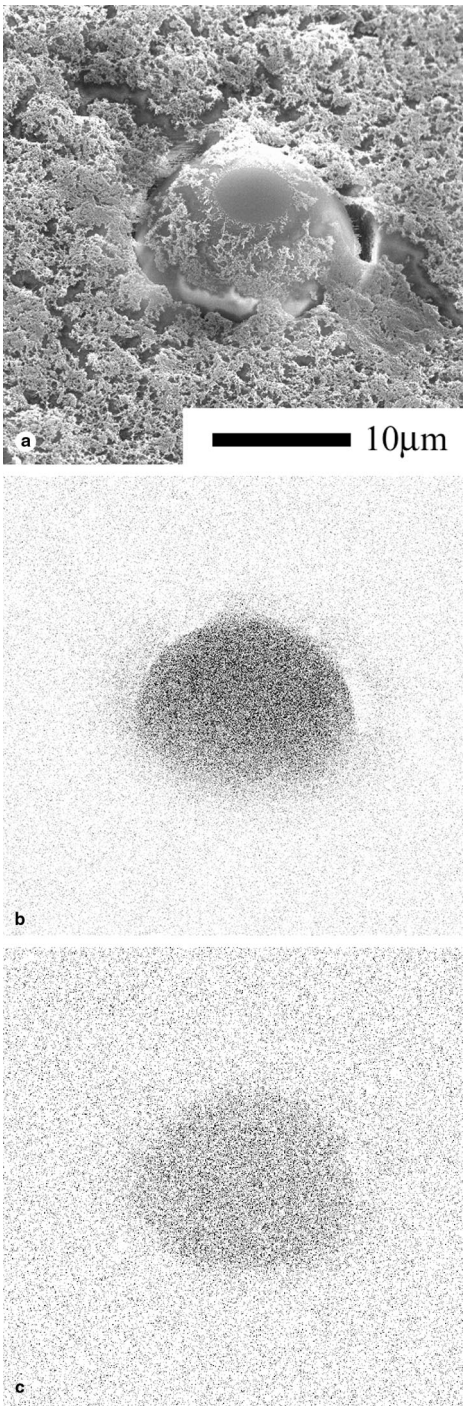

Fig. 10. (a) Phase-separated microstructure of the $SrO–B_2O_3$ system with Eu_2O_3 additions (Sample R) observed with FE-SEM; (b) and (c) Sr Lα and Eu Lα intensity maps, respectively, in the same view as (a).

the previous section. From another point of view, the behavior of Eu during the phase separation can be accounted for as follows: B_2O_3 is the common end member to the phase separation of the $RO–B_2O_3$ binary system and that of the $Eu_2O_3–B_2O_3$ binary system. Regarding the phase separation of the $RO–B_2O_3–Eu_2O_3$ ternary system as the conjugation of the phase separations of the two binary systems, it is natural for the ternary system to separate into the B_2O_3 phase and the other. It is clear that a pure B_2O_3 phase without Eu_2O_3 exists at least.

3.3. Eu concentration in the phase separation droplets

In the previous section it was shown that the Eu element dissolved preferentially in the droplets after the cooling heat-treatment to room temperature. In this section, we will discuss the concentration of Eu in the droplets and its controllability.

Fig. 11 shows a typical linear correlation between the Eu Lα signal intensity and the Eu_2O_3 content by batch in the SrO-rich end member composition. By using the calibration function, it is possible to estimate the net Eu_2O_3 content in the phase separation droplets.

Fig. 12 shows the Eu_2O_3 content by analysis in droplets after the heat-treatment of the samples R, T, V, X and Z as a function of a SrO content by batch. Although the Eu_2O_3 content by batch of each sample was fixed at 0.05 mol%, the Eu_2O_3 content by analysis in droplets varied dependent on the SrO content by batch. The Eu_2O_3 content in the droplets decreased with the increasing SrO content by batch.

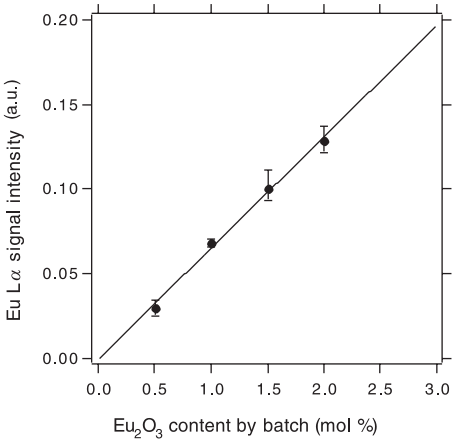

Fig. 11. Calibration function line for the Eu_2O_3 content analysis.

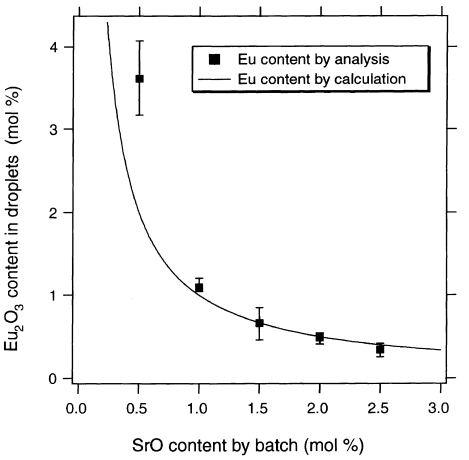

Fig. 12. Dependence of Eu_2O_3 content in droplets by analysis on the SrO content by batch in the $SrO–B_2O_3$ system with 0.05 mol% Eu_2O_3 addition. The solid line corresponds to the $y = 1/x$ function.

This tendency appears to be related to the fact that the molar ratio of two phases after completion of phase separation is determined by the batch composition. The solid line in Fig. 12 shows the ideal Eu_2O_3 content in droplets calculated from the molar ratio of two phases on the assumption that the entire Eu_2O_3 dissolved equally in each SrO-rich droplet. In this case, the sample compositions prepared may be described as $x\mathrm{SrO}\cdot(100-x)\mathrm{B_2O_3}\cdot 0.05\mathrm{Eu_2O_3}$ (mol%). Assuming the base composition of SrO-rich phase was $\mathrm{SrO}\cdot 4\mathrm{B_2O_3}$, the molar ratio of SrO-rich droplets to matrix would be $x(\mathrm{SrO}\cdot 4\mathrm{B_2O_3})\cdot 0.05\mathrm{Eu_2O_3}$ to $((100-x)-4x)\mathrm{B_2O_3}$. Scaling the Eu_2O_3 content so that the sum of the base composition of the droplets should be 100, the net Eu_2O_3 concentration is given by

$$y = 0.05\frac{100}{x+4x} = \frac{1}{x}.$$

The data reproduced well the calculated curve $y = 1/x$, indicating that the assumption was appropriate for each sample. As a result, it was found

that the Eu_2O_3 content in the droplets as a product was controllable by the batch composition under our conditions of continuous cooling.

In this study, it was found that liquid–liquid phase separation in the $RO–B_2O_3$ system is a good candidate for designing and producing glasses dispersed with Eu-enriched droplets and Eu-containing micro spheres.

4. Conclusion

The immiscibility temperatures were measured for the $PbO–B_2O_3$, $BaO–B_2O_3$ and $SrO–B_2O_3$ systems with Eu_2O_3 addition. It was found that the immiscibility temperature was increased by the addition of Eu_2O_3 in each case. The effect was more pronounced as the RO content decreased, which indicated that the nature of phase separation in the $Eu_2O_3–B_2O_3$ system became relatively dominant.

The Eu distribution map was obtained in the $RO–B_2O_3–Eu_2O_3$ phase-separated microstructure and in each phase by EPMA or FE-SEM/EDS analysis. The RO-rich droplets were enriched in Eu with a homogeneous distribution, while the matrix was almost pure B_2O_3 phase. This result was consistent with the result that the shape of the immiscibility temperature curve suggested that the ternary system dose not separate into $B_2O_3 \cdot xEu_2O_3$ and $BaO \cdot yB_2O_3 \cdot x'Eu_2O_3$ phases.

For the $SrO–B_2O_3–Eu_2O_3$ system, the net Eu_2O_3 concentration in droplets after heat-treatment was measured by EDS analysis. It was found that the Eu_2O_3 concentration in the droplets was controllable by changing the batch composition, indicating that the entire Eu_2O_3 dissolved equally in each RO-rich droplet.

Acknowledgements

This study is carried out as a part of 'Space Utilization Frontiers Joint Research Projects' promoted by National Space Development Agency of Japan (NASDA) and Japan Space Utilization Promotion Center (JSUP). We are grateful to Dr Nakamura for daily maintenance and operation of EPMA and FE-SEM/EDS.

References

[1] E.M. Levin, H.F. McMurdie, J. Am. Ceram. Soc. 32 (3) (1949) 99.
[2] R.F. Geler, E.N. Bunting, J. Res. Nat. Bur. Standard. 18 (1937) 585.
[3] E.M. Levin, G.W. Cleek, J. Am. Ceram. Soc. 41 (5) (1958) 175.
[4] Y. Ohta, K. Morinaga, T. Yanagase, Yogyo kyokai-shi 90 (1982) 511.
[5] V.B.M. Hageman, H.A.J. Oonk, Phys. Chem. Glasses 28 (5) (1987) 183.
[6] S.N. Crichton, M. Tomozawa, J. Non-Cryst. Solids 215 (1997) 244.
[7] S. Inoue, K. Wada, A. Nukui, M. Yamane, S. Shibata, A. Yasumori, T. Yano, A. Makishima, H. Inoue, M. Uo, Y. Fujimori, J. Mater. Res. 10 (6) (1995) 1561.
[8] S. Inoue, K. Wada, A. Nukui, M. Yamane, S. Shibata, A. Yasumori, T. Yano, A. Makishima, H. Inoue, K. Soga, Phys. Chem. Glasses 38 (4) (1997) 197.
[9] S. Inoue, A. Makishima, H. Inoue, K. Soga, T. Konishi, T. Asano, Y. Ishii, J. Am. Ceram. Soc. 80 (9) (1997) 2413.
[10] J.H. Simmons, J. Am. Ceram. Soc. 56 (5) (1973) 284.
[11] P.B. Macedo, J.H. Simmons, J. Res. Nat. Bur. Stand. 78A (1) (1974) 53.
[12] M. Hoch, J. Phase Equilibria 17 (4) (1996) 290.
[13] K. Nakashima, K. Hayashi, Y. Ohta, K. Morinaga, Mater. Trans. JIM 32 (1) (1991) 37.
[14] S. Inoue, A. Makishima, H. Inoue, K. Soga, T. Konishi, T. Asano, J. Non-Cryst. Solids 247 (1999) 1.
[15] Y.Z. Wang, B.L. Lu, Y.Q. Li, Y.S. Liu, Opt. Lett. 20 (7) (1995) 770.
[16] K. Miura, K. Tanaka, K. Hirao, J. Non-Cryst. Solids 213&214 (1997) 276.
[17] T. Takamori, M. Tomozawa, J. Am. Ceram. Soc. 59 (9–10) (1976) 377.
[18] S. John, G. Pang, Phys. Rev. A 54 (4) (1996) 3642.
[19] Z. Yao, Y. Ding, T. Nanba, Y. Miura, J. Ceram. Soc. Jpn. 106 (11) (1998) 1043.
[20] E.M. Levin, C.R. Robbins, H.F. McMurdie, Phase Diagrams for Ceramists, American Ceramic Society, Columbus, OH, 1969.